Available online at www.sciencedirect.com
SCIENCE DIRECT
Agricultural and Forest Meteorology 126 (2004) 117–127
AGRICULTURAL AND FOREST METEOROLOGY
www.elsevier.com/locate/agrformet

Quantification of photosynthetically active radiation inside sunlit growth chambers

Soo-Hyung Kim[a,*], Vangimalla R. Reddy[a], Jeffrey T. Baker[b], Dennis C. Gitz[c], Dennis J. Timlin[a]

[a]*Alternate Crops and Systems Laboratory, USDA-ARS, Bldg 001 Rm 342, BARC-W, 10300 Baltimore Ave., Beltsville, MD 20705, USA*
[b]*Cropping Systems Research Laboratory, USDA-ARS, Big Spring, TX 79720, USA*
[c]*Cropping Systems Research Laboratory, USDA-ARS, Lubbock, TX 79415, USA*

Received 14 November 2003; received in revised form 15 June 2004; accepted 21 June 2004

Abstract

Outdoor growth chambers allow plants to be grown under sunlight while other environmental variables such as air temperature and CO_2 concentration are controlled. Photosynthetically active radiation (PAR) inside these sunlit chambers could differ from ambient levels due to attenuations and reflections by the glazing materials. This study identified diurnal patterns and distribution of PAR inside various types of sunlit growth chambers, including soil-plant-atmosphere-research (SPAR) units using single-point and line quantum sensors. In comparison with the ambient levels, higher PAR was measured when reflections from the adjacent walls overlapped at specific locations in the SPAR unit. Within the crop growing area located in the northern part of a SPAR unit, daily integrals of PAR were between 93% and 105% of the ambient PAR on a clear day. A gradient in daily PAR existed, increasing from south to north inside the chamber. On a cloudy day, PAR within the crop growing area was between 92% and 95% of ambient PAR. A mathematical model was developed to predict incident PAR inside sunlit chambers. This model accounted for solar geometry, direct and diffuse radiations, chamber geometry, and the optical properties of the glazing material. The model was capable of simulating the diurnal patterns of PAR inside various types of sunlit chambers. The model predicted that the mean daily PAR inside sunlit chambers of acrylic sheets would usually be within 5% of the ambient PAR. Spatial distribution of the predicted daily PAR ranged from 75% to 120% of ambient levels inside various types of sunlit chambers including SPAR and open-top chambers.
Published by Elsevier B.V.

Keywords: Sunlit growth chambers; Open-top chambers; PAR; Reflectance; Transmittance; Model

1. Introduction

Controlled-environment growth chambers have been an essential tool for studying the effects of various environmental factors on plants. Several types

* Corresponding author. Tel.: +1 301 504 5343; fax: +1 301 504 5823.
E-mail address: sookim@asrr.arsusda.gov (S.-H. Kim).

0168-1923/$ – see front matter. Published by Elsevier B.V.
doi:10.1016/j.agrformet.2004.06.004

of controlled environmental chambers are widely used in plant ecophysiological research (e.g., leaf and whole-plant cuvettes, artificially lit or sunlit growth chambers, and open-top chambers). Artificially lit growth chambers may provide low light intensities and/or unrealistic light quality to plants. Recognizing the shortcomings of artificially lit growth chambers, Phene et al. (1978) designed sunlit plant growth chambers with large soil volumes known as Soil-Plant-Atmosphere-Research (SPAR) units. Since Phene et al. (1978), several other sunlit growth chambers have been constructed and utilized for studying the effects of global climate changes and for developing crop simulation models (Baker et al., 2004; Lawton et al., 1993; Liu and Walker, 1997; Pickering et al., 1994; Reddy et al., 2001; Tingey et al., 1996). These sunlit growth chambers have been a useful tool for studying canopy or small-plot responses to various combinations of environmental factors without the introduction of artifacts due to the use of artificial lighting (Liu et al., 2000). In global climate change research, sunlit growth chambers have been successfully used to identify the effects of elevated CO_2 (e.g., Baker et al., 2000). Sunlit growth chambers have also been used to investigate the interactive effects of elevated CO_2 and other environmental variables that are expected to change concomitantly such as air temperature (Allen et al., 2003), ozone (Olszyk et al., 2002), and ultraviolet (UV) radiation (Zhao et al., 2003).

Sunlit growth chambers have been built with various designs and materials. Materials with high optical clarity such as Plexiglas (Reddy et al., 2001; Baker et al., 2004), Teflon film and Plexiglas (Tingey et al., 1996), Mylar (Pickering et al., 1994), and polycarbonate (Liu and Walker, 1997) were used as above-ground compartment materials. Depending upon the materials used to build the chamber enclosure, quality of light inside the chamber could be different from the outside. For instance, some materials (e.g., Plexiglas) do not transmit short wavebands (e.g., UV). This difference in light quality between inside and outside the sunlit chambers has been recognized (Liu et al., 2000; Tingey et al., 1996).

Solar incidence angles with respect to a stationary glazing surface vary throughout the day and year, resulting in variable transmissions and reflections of radiation by the surface. Variable transmissions and heterogeneity of solar radiation inside greenhouses due to greenhouse geometry, structural elements, solar positions, and the optical properties of glazing materials have been recognized and studied (Critten and Bailey, 2002). A number of experimental and theoretical studies have focussed on quantification of solar radiation inside various types of greenhouses (Critten, 1983; De Zwart, 1993; Kozai, 1977; Thomas, 1978; Wang and Boulard, 2000). In contrast, the quantity and distribution of solar radiation inside the sunlit growth chambers have not been well studied to date.

This paper reports the experimental identification of diurnal patterns, distribution, and daily integrals of PAR inside the sunlit growth chambers, and presents a mathematical model that takes into account variable transmissions and reflections of PAR by the chamber walls using a simple ray tracing algorithm to quantitatively characterize the PAR environment inside the sunlit chambers.

2. Materials and methods

2.1. Soil-plant-atmosphere-research (SPAR) units

The outdoor, sunlit, controlled-environment chambers used in this study are located at the USDA-ARS, Alternate Crops and Systems Laboratory in Beltsville, MD, USA (39° 0′ N, 76° 6′ W). The chambers are of two types, referred to here as either 'SPAR' (Soil-Plant-Atmosphere-Research, 12 chambers) or 'Daylit' (6 chambers). This facility is comparable in design and operation to the systems at the University of Florida (Pickering et al., 1994), Corvallis, Oregon (Tingey et al., 1996) and Mississippi State University (Reddy et al., 2001). The SPAR chambers consist of transparent chamber tops constructed of 0.0127 m thick clear acrylic sheet. This chamber top has the dimensions of 2.2 m × 1.4 m × 2.5 m (length × width × height) (Fig. 1A and B). The acrylic sheet has a refractive index of 1.491, total transmittance of approximately 92%, reflectance of 4% for each side, and absorption of less than 0.2% per cm of thickness for rays in PAR wavebands normal to the sheet (Plexiglas G[1], Atoglas-ATOFINA chemicals, Inc., Philadelphia, PA, USA). Each SPAR chamber top is mounted to a steel soil bin measuring

[1] Mention of this or other proprietary products is for the convenience of the readers only, and does not constitute endorsement or preferential treatment of these products by USDA-ARS.

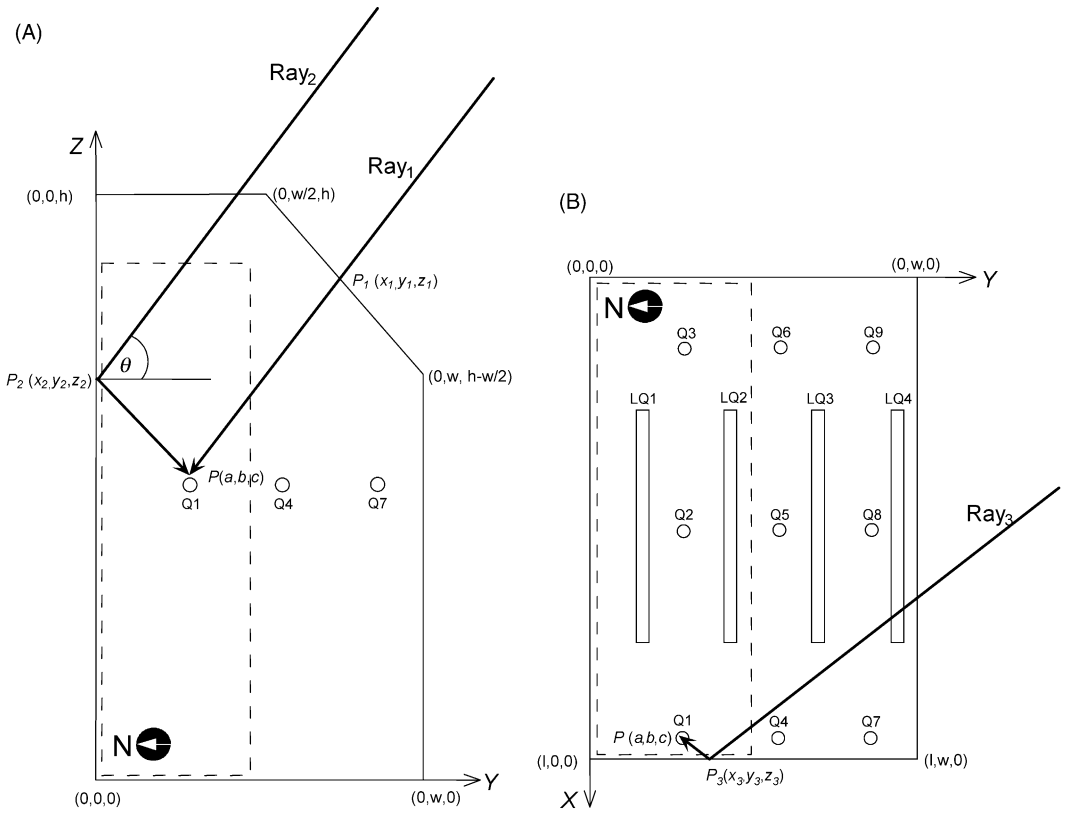

Fig. 1. Schematic diagram of a SPAR chamber and locations of point quantum (Q1–Q9) and line quantum (LQ1–LQ4) sensors within the chamber. A: View from west; B: view from above. $P(a, b, c)$ is a point inside the chamber. The model accounts for three rays intersecting at point P (Ray_1, Ray_2, and Ray_3: see text for details of the model). θ is the angle between a ray and the vector normal to a chamber wall. Length (l = 2.2 m) and width (w = 1.4 m) of the chamber were defined in east-west direction (x-axis) and in north-south direction (y-axis), respectively. Height (h = 2.5 m) was defined in z-direction. Area inside the dashed line corresponds to crop growing area in the SPAR chamber. All Q and LQ were placed at a height of 1.4 m.

2.2 m × 0.6 m × 1.0 m (length × width × depth). The surface of this soil bin corresponds to the crop growing area (the northern half of total chamber area) in the SPAR units (Fig. 1B). The Daylit chambers are constructed of the same acrylic sheet, and are 2.3 m tall with an interior raised bench 0.5 m above the floor of the chamber. Each chamber has a cross-sectional area of 1.2 m^2 with a total chamber volume of 3,360 L (Fig. 2). Further details of SPAR and Daylit chambers, and their operation are described in Baker et al. (2004).

2.2. PAR distribution inside a SPAR unit: observations and modeling

Nine single-point quantum sensors (LI-190SA, Li-Cor, Lincoln, NE, USA) and four line quantum sensors (LI-191SA, Li-Cor, Lincoln, NE, USA) were positioned inside a SPAR chamber and connected to a data logger to measure and record PAR (Fig. 1A and B). Hereafter, quantum sensors and line quantum sensors were denoted using Q and LQ, respectively. LQ1, LQ2, LQ3, and LQ4 were oriented in an east-west direction and located at 1.1 m, 0.8 m, 0.4 m, and 0.1 m from the south wall, respectively. All sensors were raised to a height of 1.4 m and leveled with a bubble site. An additional point and line quantum sensors were placed outside the chamber to simultaneously measure ambient PAR.

Diurnal patterns of PAR were monitored on a cloudy day (April 26, 2003) and a clear day (April 27, 2003). The proportion of diffuse radiation in Beltsville, MD, was over 95% throughout most of

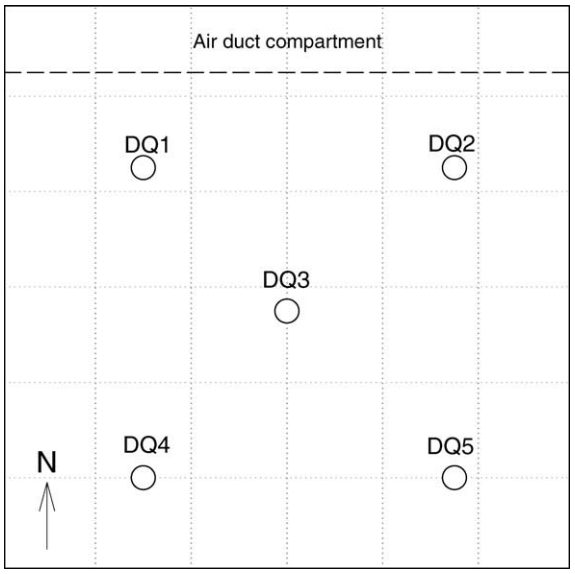

Fig. 2. Schematic diagram of a Daylit chamber viewed from above and locations of quantum sensors (DQ1–DQ5) used for model validation experiment inside the chamber. All sensors were placed at 0.5 m from the bench.

the day on April 26, while it was around 15% near solar noon on April 27, determined with a shadowband radiometer (Model MFR-7, Yankee Environmental Systems, Turners Falls, MA, USA) operated by the USDA UV-B monitoring and research program (http://uvb.nrel.colostate.edu/UVB/uvb_climate_network.html).

A mathematical model was developed to predict PAR inside the SPAR chamber. This model took into account the optical properties of the chamber walls, chamber dimensions, and solar geometry. Chamber dimensions were described by length, width, height and a diagonal side (Fig. 1A). A point P within the chamber was expressed using the Cartesian coordinates originating from the north-east corner at the soil surface. Total ambient PAR (I_0) was input into the model. This value was partitioned into direct and diffuse portions. Based on the approximation of direct and diffuse radiations by Cambell and Norman (1998), the direct portion of ambient PAR (I_{0dr}) was estimated from total ambient PAR (I_0) as:

$$I_{0dr} = \left(\frac{\tau_a^m}{\tau_a^m + 0.3(1-\tau_a^m)}\right) I_0 \quad (1)$$

where τ_a is the atmospheric transmittance, and m is the optical air mass number estimated using:

$$m = \frac{p_a}{101.3 \sin\beta} \quad (2)$$

where p_a is atmospheric pressure in kPa, 101.3 accounts for sea level atmospheric pressure in kPa, and β is solar elevation angle. Total ambient PAR (I_0) was either measured using quantum sensors or estimated by accounting for sun angles and day length as described by Campbell and Norman (1998). Diffuse ambient PAR (I_{0df}) was then estimated by subtracting I_{0dr} from I_0. Using this relationship, clear and overcast sky were simulated by applying $\tau_a = 0.6$ and $\tau_a = 0.0$, respectively.

Three rays falling onto a point P (a, b, c) inside the chamber were traced (A ray was defined as a line): (1) A ray that enters the chamber through a point (P_1) on a side of the chamber (Ray_1 in Fig. 1A); (2) the other ray reflected from a point (P_2) in the chamber north wall (Ray_2 in Fig. 1A); (3) the third ray reflected from a point (P_3) in either east or west wall (Ray_3 in Fig. 1B). The Cartesian coordinates of point P_1 (x_1, y_1, z_1) through which a ray entered the chamber to reach point P (a, b, c) inside the chamber was identified as:

$$\begin{pmatrix} x_1 \\ y_1 \\ z_1 \end{pmatrix} = \begin{pmatrix} a \\ b \\ c \end{pmatrix} + t_1 \begin{pmatrix} \sin\psi \\ \cos\psi \\ \tan\beta \end{pmatrix} \quad (3)$$

where ψ is solar azimuth in radians reading south zero (solar noon) and east negative (morning). Parameter t_1 was determined by identifying the chamber wall that a ray intersected. For example, if a ray intersected the east wall of the chamber (yz-plane in Fig. 1B) then setting $x_1 = 0 = a + t_1 \times \sin\psi$, we obtained $t_1 = -a/\sin\psi$. Point P_2 (x_2, y_2, z_2) was identified as the intersection between the reflected ray passing through P and the north wall:

$$\begin{pmatrix} x_2 \\ y_2 \\ z_2 \end{pmatrix} = \begin{pmatrix} a \\ b \\ c \end{pmatrix} + t_2 \begin{pmatrix} \sin(-\psi) \\ \cos(-\psi) \\ \tan(-\beta) \end{pmatrix} \quad (4)$$

Here, parameter t_2 was defined as $-b/\cos(-\psi)$ resulting in $y_2 = 0$. Likewise, P_3 (x_3, y_3, z_3) was found

by the following relationship.

$$\begin{pmatrix} x_3 \\ y_3 \\ z_3 \end{pmatrix} = \begin{pmatrix} a \\ b \\ c \end{pmatrix} + t_3 \begin{pmatrix} \sin(-\psi) \\ \cos(-\psi) \\ \tan\beta \end{pmatrix} \quad (5)$$

The parameter t_3 was determined by $(l - a)/\sin(-\psi)$ resulting in $x_3 = l$ and by $-a/\sin(-\psi)$ resulting in $x_3 = 0$ for morning and afternoon, respectively. Lastly, l is the length of chamber in x-direction. Once P_2 and P_3 were identified, rays transmitting to these points were identified similarly as done for P_1 of Ray_1.

The angle (θ) between an incident ray and the vector normal to a plane of the transmitting or reflecting wall was calculated by using the vector dot product. Thus, θ was defined as a function of ψ and β. Transmittance (τ), reflectance (ρ) and absorptance (α) of a ray by a chamber wall was calculated as a function of θ according to Takakura (1993). A ray incident on a clear sheet is partly reflected at the surface and the rest is refracted. Due to successive internal reflections within the glazing sheet, transmitted, reflected, and absorbed ray components can be expressed as the sums of infinite series of each reflected component. Thus, calculations of τ, ρ, and α were made taking into account refracted angle, extinction coefficient and thickness of the acrylic sheet, infinite series of internal reflections, and incident angle of the ray. A detailed description of these calculations was given by Takakura (1993). Based on the manufacturer's specification, an extinction coefficient (k) of $1.97 \times 10^{-4}\,\text{mm}^{-1}$ was used in the calculations of τ, ρ, and α.

After taking into account τ, ρ, and α by the chamber walls, the remainders of the three rays were added to represent the fraction of PAR incident on point P:

$$F_{\text{PAR}} = \tau_1 + \tau_2\rho_2 + \tau_3\rho_3 \quad (6)$$

where τ_1, τ_2, and τ_3 represent the transmittance through corresponding chamber walls for Ray_1, Ray_2, and Ray_3, respectively. Reflectance from the north wall and either side wall are ρ_2 and ρ_3, respectively. Thus, the direct portion of PAR incident on point P ($I_{\text{P\_dr}}$) was represented by:

$$I_{\text{P\_dr}} = I_{0\text{dr}} F_{\text{PAR}} \quad (7)$$

As diffuse radiation comes from all directions in the upper hemisphere, diffuse PAR to the point P ($I_{\text{P\_df}}$) for a uniform overcast sky was calculated from:

$$I_{\text{P\_df}} = \frac{I_{0\text{df}}}{\pi} \int_{-\pi}^{\pi} \int_{0}^{\pi/2} F_{\text{PAR}} \sin\beta \cos\beta \, \text{d}\beta \, \text{d}\psi \quad (8)$$

Because F_{PAR} is a function of τ and ρ that depend on ψ and β through θ, the integration over the solid angle of the upper hemisphere in Eq. (8) was carried out numerically using the Gauss integration method (Hildebrand, 1974; Röhrig et al., 1999).

A computer simulation model was developed based on the mathematical relationships described above. Diurnal patterns and daily integral of PAR inside the SPAR chamber were simulated using the model. To verify the model predictions, ambient PAR measured outside the chambers was used as input and results were compared with PAR measured inside a SPAR chamber using the quantum sensors (Fig. 3). In addition, daily integration of PAR (daily PAR) was simulated on every 10 cm^2 grid inside a SPAR chamber. Horizontal distribution of this simulated daily PAR was determined at 0.5, 1.0 and 1.5 m from the soil surface (Fig. 4). Ambient solar radiation was modeled according to Campbell and Norman (1998), and was used as input to simulate PAR inside the chamber. The results were expressed as proportions of ambient PAR (i.e., if 10% higher than the ambient, it was 1.1). Daily PAR was simulated for April 30, 2003. All simulations were run for Beltsville (39° 0′ N, 76° 6′ W), MD, USA. Symbols used in the model and their description are listed in Appendix A.

2.3. Model validation and application to daylit and open-top chambers

To validate the model predictions, PAR inside a Daylit chamber was measured using five quantum sensors (DQ1–DQ5 in Fig. 2) for July 3–6, 2003. One quantum sensor was positioned in the centre and the other four were placed in each inside corner of a Daylit chamber (Fig. 2). All sensors were raised to 0.5 m from the bench. Diurnal patterns and daily PAR were measured and compared with the model predictions. The observed and predicted values of daily PAR inside the Daylit chamber were expressed as a proportion of the ambient daily PAR falling on to a horizontal surface (Fig. 5C). The model performance was evaluated by linear regression of the predicted

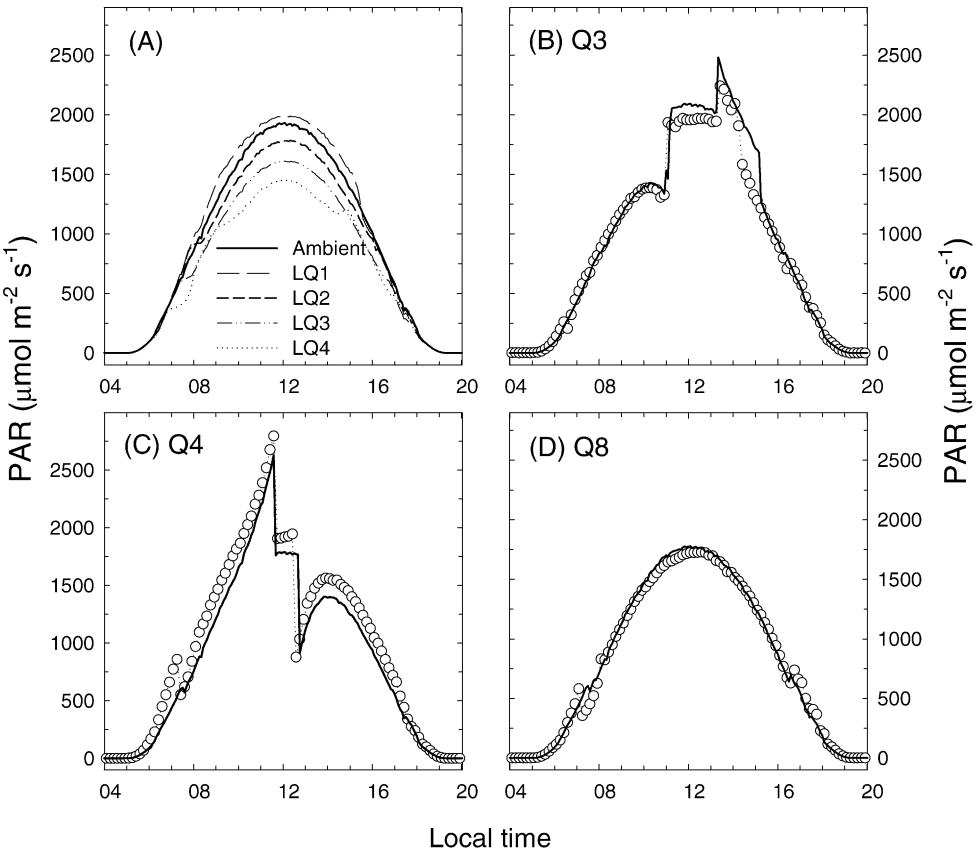

Fig. 3. Diurnal patterns of PAR inside a SPAR chamber (clear sky). A: PAR measured using line quantum sensors (LQ1–LQ4) on April 27, 2003. The solid line represents ambient PAR values. B: Measured and predicted PAR at Q3; C: measured and predicted PAR at Q4; D: measured and predicted PAR at Q8. Circles are measured PAR and lines represent model predictions.

daily PAR on the observed daily PAR inside the chamber. Significance of the linear regression, r^2, slope unity, and zero intercept were tested. Bias and root mean square error (RMSE) were also evaluated as measures of the model performance (Retta et al., 1991).

The model was used to decompose the diurnal patterns of PAR at Q1 in the SPAR unit into each ray component (i.e., Ray_1, Ray_2, and Ray_3 of direct PAR, and diffuse PAR) for a clear sky (April 30). The model was also used to simulate PAR inside an open-top chamber (i.e., 100% transmission through the ceiling). It was assumed that the open-top chamber was of the same dimensions as the Daylit chamber. This simulation was run for a clear sky (July 5) at a height of 0.5 m.

3. Results

3.1. Diurnal patterns and distribution of PAR inside a SPAR chamber

Data obtained from the line quantum sensors suggested that for clear sky conditions PAR near the north wall (LQ1) was higher than ambient PAR, whereas PAR near the south wall (LQ3 and LQ4) was lower than the ambient PAR (Fig. 3A). A PAR gradient existed within each SPAR chamber (increasing from south to north). LQ1 through LQ4 received 104.6%, 93.1%, 83.4%, and 76.4% of daily ambient PAR, respectively.

For a clear sky, diurnal PAR results obtained from Q1, Q4, and Q7 showed that these sensors received

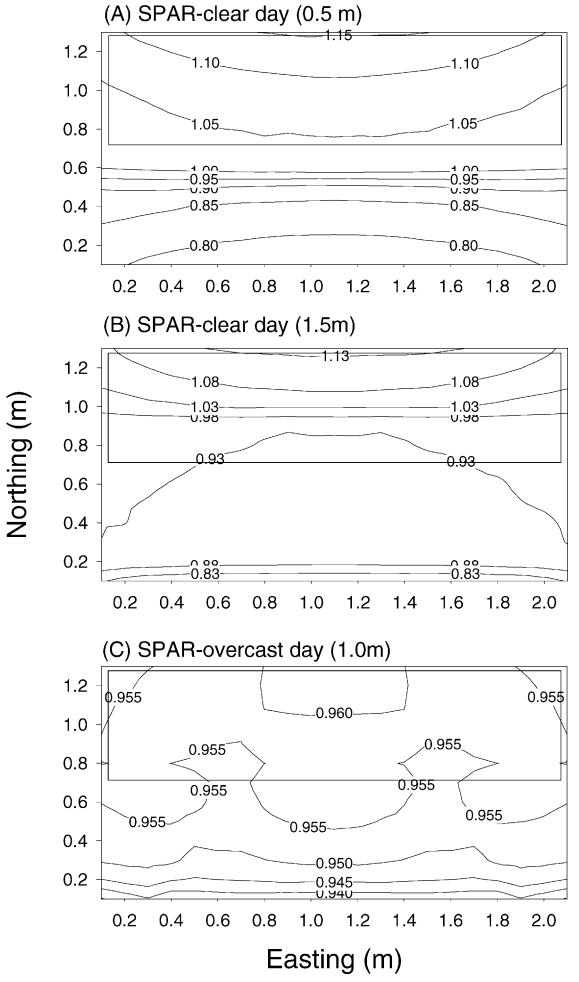

Fig. 4. Simulated daily PAR inside a SPAR chamber in relation to ambient PAR. Simulations were run for April 30. Area inside the grey rectangle corresponds to crop growing area. The contour lines indicate daily PAR levels. The daily PAR was expressed as proportions of the ambient daily PAR. A: Daily PAR at 0.5 m from the soil surface (clear sky); B: daily PAR at 1.5 m from the soil surface (clear sky); C: daily PAR at 1.0 m from the soil surface (overcast sky).

higher PAR than outside the chamber in the morning, exhibiting a spike followed by an abrupt drop just before noon. The point quantum sensors located close to the south wall (Q7–Q9) logged lower PAR than the ambient throughout the day (Fig. 3D). The model developed in this study was capable of simulating the patterns and magnitudes of light distribution inside a SPAR chamber very closely (Fig. 3B–D; solid lines). Those sensors located inside the crop growing area (Q1–Q3 and LQ1–LQ2) received higher or similar PAR than the outside.

For an overcast sky, the diurnal course of PAR inside the SPAR chamber was evenly distributed and was close to ambient PAR throughout the day. This was evident as LQ1 through LQ4 received 94.9%, 92.1%, 88.0%, and 88.8% of ambient daily PAR, respectively (data not shown). Data obtained from the point quantum sensors showed similar patterns to data from the line quantum sensors under overcast sky conditions. Setting $\tau = 0$ to simulate overcast sky, the model predictions for PAR at any locations inside the SPAR chamber were similar to the ambient PAR.

3.2. Simulation of daily PAR inside a SPAR chamber

At 0.5 m from the soil surface, the simulated daily PAR near the north wall was up to 10% higher than the ambient daily PAR under a clear sky (Fig. 4A). For the area close to the south wall, the simulated daily PAR was up to 20% lower than the ambient values. At 1.5 m from the soil surface, the simulated daily PAR spanned from 80% to 113% of ambient PAR (Fig. 4B). For a clear sky, the model predicted that the crop growing area in the SPAR chamber (Fig. 1B) received higher daily PAR than the ambient at either height (Fig. 4A and B). For an overcast sky, most areas in the SPAR chamber, including the crop growing area, were found to receive near 94–96% of ambient PAR at 1.0 m from the soil surface (Fig. 4C).

Mean daily PAR across the entire horizontal surface area or the crop growing area of a SPAR chamber was estimated and compared with the ambient daily PAR. For clear sky conditions and a height of 0.5 m, the entire area received 97.9% of ambient daily PAR on average, while the crop growing area received 107.8% of the ambient PAR. At a height of 1.5 m, mean daily PAR for the entire area and the crop growing area were 96.2% and 101.6% of the ambient PAR, respectively. For an overcast sky and a height of 1.0 m, these numbers were 94.8% and 95.3% of the ambient PAR, respectively.

3.3. Model validation and application

Diurnal patterns of observed PAR inside a Daylit chamber for overcast (July 3) and mostly clear (July 4) skies compared well with the model predictions

(Fig. 5A and B). For an overcast sky, diurnal patterns of PAR inside the chamber were similar to the ambient PAR regardless of the sensor locations (Fig. 5A). For a mostly clear sky, the sensors located close to the north wall showed higher PAR than the ambient values (Fig. 5B). The model was capable of simulating the observed diurnal patterns reasonably well inside the Daylit chamber for overcast and clear skies.

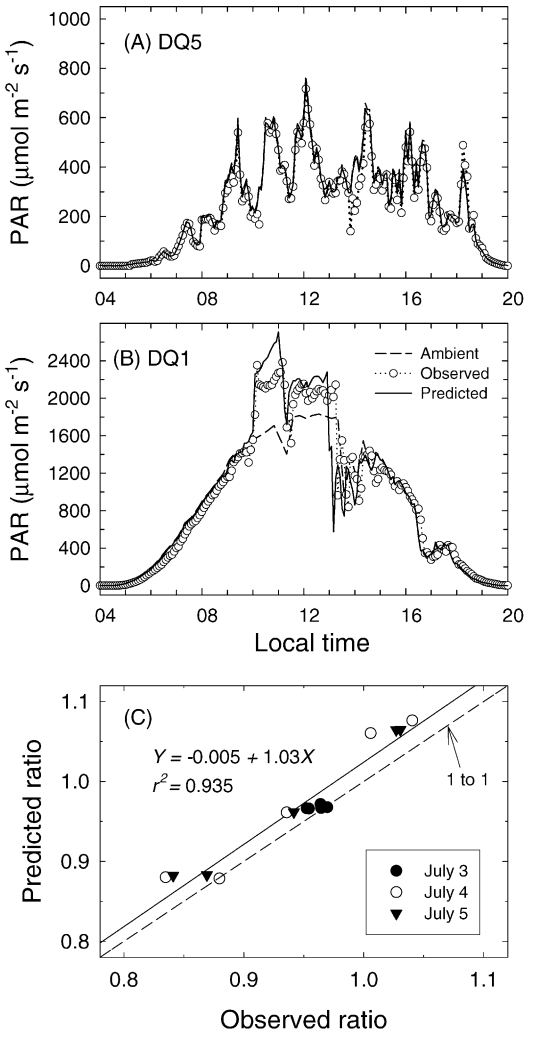

Fig. 5. Model validation with a Daylit chamber. A: Diurnal patterns of ambient (dashed line), measured (circles), and predicted (solid line) PAR at DQ5 (July 3; overcast sky); B: diurnal patterns of PAR at DQ1 (July 5; clear sky); C: linear regression of predicted daily PAR on measured daily PAR for all five sensors (July 3–5). Values were expressed as proportions of the ambient daily PAR.

For clear sky conditions, observed daily PAR inside the Daylit chamber ranged between 83% and 104% of the ambient values. Locations DQ1 and DQ2 received higher daily PAR than the ambient, while DQ4 and DQ5 exhibited lower than the ambient values. For an overcast sky, all five locations received between 94% and 97% of the ambient daily PAR. Regression analysis of the model performance indicated that: (1) model was capable of identifying the distribution of daily PAR inside the Daylit chamber as the slope and intercept of regression that were not different from unity ($P = 0.704$) and zero ($P = 0.948$), respectively, and $r^2 = 0.935$ (Fig. 5C); (2) model slightly overestimated daily PAR as bias and RMSE of the model predictions were +2.28% and 2.32% of the observed values, respectively.

Diurnal patterns of each ray component (i.e., Ray_1, Ray_2, and Ray_3) of direct PAR were shown along with ambient, diffuse and total PAR for location Q1 (see Fig. 1) inside a SPAR chamber for a clear sky (Fig. 6A). This illustrates that the spike between 9:00 and 12:00 was due to two overlapping reflections from the north and west chamber walls.

With an open-top chamber under clear sky conditions, daily PAR was predicted to range between 75% and 120% with a gradient from south to north at 0.5 m from the soil surface (Fig. 6B). The model predicted that open-top chambers would transmit 3% to 6% more daily PAR than closed chambers with the same dimensions owing to the absence of the chamber ceiling. The model predicted that average daily PAR inside the open-top chamber was 99% of ambient daily PAR at 0.5 m for a clear day.

4. Discussion

In sunlit chamber studies, variability of PAR inside the chambers is often not explicitly examined but the transmittance of the glazing material specified by manufacturer or a single point measurement of PAR within a chamber is used to estimate PAR at the top of the canopy. Depending on the location of the sensor, PAR readings at the top of the canopy can be different from ambient PAR. For example, some readings of the PAR sensors located in the north-west corner (e.g., Q1, Q4) reached over 2500 $\mu mol\ m^{-2}\ s^{-1}$ just before noon followed by an abrupt drop in the present study

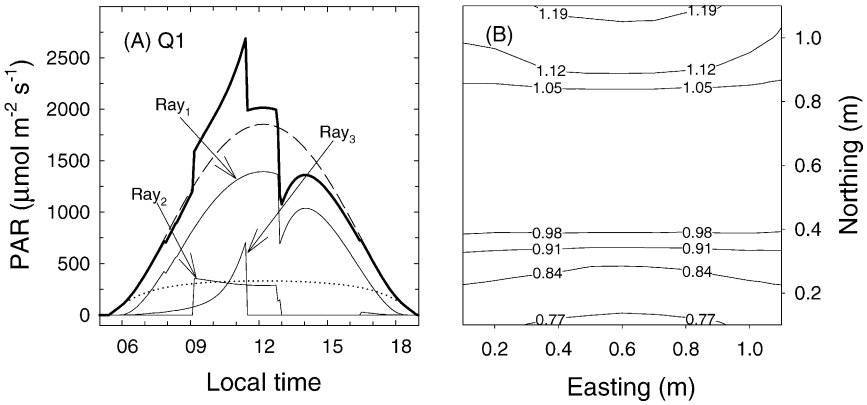

Fig. 6. Model applications. A: Simulated diurnal patterns of PAR at Q1 in SPAR chamber (April 30; clear sky). Total PAR (thick solid line) at Q1 was decomposed to Ray_1, Ray_2 and Ray_3 of direct PAR (thin solid lines), and total diffuse PAR (dotted line) using the model, and compared with the ambient PAR (dashed line); B: simulation of daily PAR inside an open-top chamber at 0.5 m from the soil surface for a clear day (July 5). The same dimensions as the Daylit chamber were assumed. Daily PAR was expressed as proportions of the ambient daily PAR.

(Fig. 3C and Fig. 6A). Typically, maximum ambient PAR of around 2000 μmol m^{-2} s^{-1} is observed in this region in the summer. PAR data obtained from LQ1, Q1, Q2, and Q3 indicated that locations close to the north wall received higher PAR than outside due to reflections mainly from the north wall. The locations adjacent to the south wall received lower PAR than the outside on a clear day (Fig. 3). This is because little reflected rays were available near the south wall. In addition, transmittance was low through the south wall when β was high. When β is high, both τ through the ceiling or diagonal side and ρ from the vertical walls (e.g., north or south wall) are high. At some instances, a transmitted ray through either the flat ceiling or the diagonal side and two reflected rays from the adjacent walls converge onto a spot in the corner. This results in acute spikes observed in this experiment (Fig. 3B and C) as illustrated by the model output of each ray component (Fig. 6A). Because α, ρ, and τ are a function of θ, they vary over time of the day, as well as day of the year. This accounts for the fact that some locations (e.g., Q1) in the chamber under clear sky receive a different diurnal PAR pattern than the ambient throughout the day.

Given a uniform overcast sky, the diurnal pattern of PAR inside sunlit chambers would be similar to the ambient conditions because direct radiation is negligible or absent. The diffuse radiation, which comes from all directions of the hemisphere, would result in an even distribution inside the chamber. In this case there would be no or little overlapping specular reflections of direct beams. With the reflected components (Ray_2 and Ray_3) excluded in the simulations (i.e., only Ray_1 from all angles was accounted for), the model predicted that mean diffuse PAR inside the chambers was near 85% of the ambient diffuse PAR regardless of the chamber type (data not shown). This agrees with the manufacturer's description that for a uniform overcast sky, the transmittance of acrylic sheet will be approximately 85%. In addition, the model predicted that the reflected components of diffuse PAR (i.e., sum of Ray_2 and Ray_3 from all angles) were near 10% of the ambient diffuse PAR, resulting in total diffuse PAR inside the chambers to be near 95% of the ambient diffuse PAR at 0.5 m from the soil surface.

While the model predicted the diurnal patterns of instantaneous PAR well in comparison with the measured values (Fig. 5A and B), it slightly overestimated daily PAR for Daylit chambers (Fig. 5C). One possible reason for this is that there are factors (i.e., weathering, scratches or dirt/dusts) that alter the optical properties of the glazing materials. These factors might have lowered the clarity of the material and resulted in lower transmittance of solar radiation than the original specification, whereas the model assumed the same optical properties as originally specified by manufacturer.

On an average, the model predicted that all three types of the chambers would transmit over 90% of the ambient PAR. For the SPAR chambers, mean daily

PAR over the crop growing area (the northern half of total chamber area: see Fig. 1B) was predicted to be higher (up to 9%) than ambient PAR during clear sky conditions. These predictions and measurements of PAR within the sunlit chambers indicate that the distribution of PAR inside the chamber could be fairly heterogeneous, while the spatial mean of total PAR remains similar to ambient PAR. When studying plant species that are sensitive to variations in PAR, the variability of PAR inside sunlit chambers should be carefully considered. A pattern that was consistent among different types of sunlit chambers was the gradient in daily PAR from the south to north end of the chamber. This suggests some practical sampling tactics. For example, if a treatment is to be imposed on different plants within chambers, blocks can be used in an east-west direction to minimize the confounding effects of the PAR gradient inside the chamber. Typically, shade cloths are used to surround plant canopy in sunlit growth chamber studies. These shade cloths are raised daily to the canopy height to minimize the edge effect. It should be noted that if no shade cloths were used, plants near the chamber walls would receive higher PAR as border plants than the rest.

5. Conclusions

The average density of PAR inside the sunlit chambers was close to ambient PAR while distribution of daily PAR was heterogeneous on clear days. It is believed that this was due to varying transmissions and reflections from the chamber tops and walls as a function of the angle between incident rays and chamber walls. A mathematical model was developed to identify the diurnal patterns of incident PAR and to quantify the distribution of the daily integrated PAR inside sunlit chambers. Using the model, it was found that daily PAR varied over locations within the chamber, exhibiting a pattern increasing from south to north inside the chamber. The results of this study can be applied to chamber experiments where plants and/or sampling regimes are sensitive to short-term spatial or temporal variations in PAR. The model developed in this study can be useful for comparing and quantifying PAR received inside sunlit growth chambers with various designs and glazing materials. The model may also be useful for designing sunlit chambers with minimal internal PAR variations.

Acknowledgements

We thank Jackson Fisher, Robert Jones, and Emily Warnock for their valuable assistance. We thank Drs. M.S. Kim, L.H. Allen Jr., K.R. Reddy, and anonymous reviewers for helpful and constructive comments on the manuscript.

Appendix A. Symbols used in this paper

Symbol	Units	Description
a	–	x coordinate of point P
b	–	y coordinate of point P
c	–	z coordinate of point P
F_{PAR}	–	Fraction of PAR intersecting point P
I_0	μmol m^{-2} s^{-1}	Total ambient PAR
I_{0df}	μmol m^{-2} s^{-1}	Diffuse portion of I_0
I_{0dr}	μmol m^{-2} s^{-1}	Direct portion of I_0
I_{P_df}	μmol m^{-2} s^{-1}	Diffuse PAR incident on point P
I_{P_dr}	μmol m^{-2} s^{-1}	Direct PAR incident on point P
m	–	Optical air mass number
P	–	Point (a, b, c) inside a chamber
P_1	–	Point through which Ray_1 enters the chamber
P_2	–	Point on either north or south wall from which Ray_2 reflects
P_3	–	Point on either east or west wall from which Ray_3 reflects
p_a	kPa	Atmospheric pressure
Ray_1	–	Ray entering the chamber through point P_1intersecting point P
Ray_2	–	Ray reflecting from point P_2
Ray_3	–	Ray reflecting from point P_3
t_i	–	Scalar multiplier for vector PP_i (i = 1,2 or 3)
x_i	–	x coordinate of point P_i (i = 1,2 or 3)
y_i	–	y coordinate of point P_i (i = 1,2 or 3)
z_i	–	z coordinate of point P_i (i = 1,2 or 3)
α	–	Absorptance of a chamber wall
β	radian	Solar elevation
θ	radian	Angle between a ray and the normal vector of a chamber wall
ρ_i	–	Reflectance of a chamber wall for Ray_i (i = 1,2 or 3)
τ_i	–	Transmittance of a chamber all for Ray_i (i = 1,2 or 3)
τ_a	–	Atmospheric transmittance
ψ	radian	Solar azimuth (south = 0, east= $-\pi/2$, west = $\pi/2$)

References

Allen Jr., L.H., Pan, D., Boote, K.J., Pickering, N.B., Jones, J.W., 2003. Carbon dioxide and temperature effects on evapotranspiration and water use efficiency of soybean. Agron. J. 95, 1071–1081.

Baker, J.T., Allen Jr., L.H., Boote, K.J., Pickering, N.B., 2000. Direct effects of atmospheric carbon dioxide concentration on whole canopy dark respiration of rice. Global Change Biol. 6 (3), 275–286.

Baker, J.T., Kim, S.-H., Gitz, D.C., Timlin, D., Reddy, V.R., 2004. A method for estimating carbon dioxide leakage rates in controlled-environment chambers using nitrous oxide. Environ. Exp. Botany 51 (2), 103–110.

Critten, D.L., 1983. A computer model to calculate the daily light integral and transmissivity of a greenhouse. J. Agric. Eng. Res. 28 (1), 61–76.

Critten, D.L., Bailey, B.J., 2002. A review of greenhouse engineering developments during the 1990s. Agric. For. Meteorol. 112 (1), 1–22.

De Zwart, H.F., 1993. Determination of direct transmission of a multispan greenhouse using vector algebra. J. Agric. Eng. Res. 56 (1), 39–49.

Hildebrand, F.B., 1974. Introduction to numerical analysis, McGraw-Hill, New York.

Kozai, T., 1977. Direct solar light transmission into single-span greenhouses. Agric. Meteorol. 18 (5), 327–338.

Lawton, J.H., Naeem, S., Woodfin, R.M., Brown, V.K., Gange, A., Godfray, H.J.C., Heads, P.A., Lawler, S., Magda, D., Thomas, C.D., Thompson, L.J., Young, S., 1993. The Ecotron: a controlled environmental facility for the investigation of population and ecosystem processes. Philos. Trans. R. Soc. London, B Biol. Sci. 341 (1296), 181–194.

Liu, L., Hoogenboom, G., Ingram, K.T., 2000. Controlled-environment sunlit plant growth chambers. Crit. Rev. Plant Sci. 19 (4), 347–375.

Liu, L., Walker, P.N., 1997. A damper-controlled sunlit growth chamber with independent control of root temperature. Trans. ASAE 40 (6), 1677–1683.

Olszyk, D., Tingey, D., Wise, C., Davis, E., 2002. CO_2 and O_3 alter photosynthesis and water vapor exchange for *Pinus ponderosa* needles. Phyton-Annales Rei Botanicae 42 (3), 121–134.

Phene, C.J., Baker, D.N., Lambert, J.R., Mckinion, J.M., 1978. SPAR—a soil-plant-atmospheric research system. Trans. ASAE 23, 589–595.

Pickering, N.B., Allen, L.H.J., Albrecht, S.L., Jones, P., Jones, J.W., Baker, J.T., 1994. Environmental plant chambers: control and measurement using cr-10 data loggers. In: Watson, D.G., Zazueta, F.S., Harrison, T.V. (Eds.), Computers in Agriculture. Proceedings of the 5th International Conference. American Society of Agricultural Engineers, St. Joseph, Michigan 49845, Orlando, Florida, USA, Feb. 5–9, pp. 29–35.

Reddy, K.R., Hodges, J.J., Read, J.J., McKinion, J.M., Baker, J.T., Tarpley, L., Reddy, V.R., 2001. Soil-Plant-Atmosphere-Research (SPAR) facility: a tool for plant research and modeling. Biotronics 30, 27–50.

Retta, A., Vanderlip, R.L., Higgins, R.A., Moshier, L.J., Feyerherm, A.M., 1991. Suitability of corn growth models for incorporation of weed and insect stresses. Agron. J. 83 (4), 757–765.

Röhrig, M., Stützel, H., Alt, C., 1999. A three-dimensional approach to modeling light interception in heterogeneous canopies. Agron. J. 91, 1024–1032.

Thomas, R.B., 1978. The use of specularly-reflecting back walls in greenhouses. J. Agric. Eng. Res. 23 (1), 85–97.

Tingey, D.T., McVeety, B.D., Waschmann, R., Johnson, M.G., Phillipps, D.L., Rygiewicz, P.T., Olszyk, D.M., 1996. A versatile sun-lit controlled-environment facility for studying plant and soil processes. J. Environ. Qual. 25 (3), 614–625.

Wang, S.J., Boulard, T., 2000. Measurement and prediction of solar radiation distribution in full-scale greenhouse tunnels. Agronomie 20 (1), 41–50.

Zhao, D., Reddy, K.R., Kakani, V.G., Read, J.J., Sullivan, J.H., 2003. Growth and physiological responses of cotton (gossypium hirsutum l.) to elevated carbon dioxide and ultraviolet-b radiation under controlled environmental conditions. Plant Cell Environ. 26 (5), 771–782.